JETIR.ORG ISSN: 2349-5162 | ESTD Year : 2014 | Monthly Issue
JOURNAL OF EMERGING TECHNOLOGIES AND INNOVATIVE RESEARCH (JETIR)
An International Scholarly Open Access, Peer-reviewed, Refereed Journal

Computational Investigation of Advanced Winglet Configurations for Enhanced Aircraft Aerodynamic Performance

S. Pravinkumar[1], Gutlapalli Virinchi Hrushikesa Koumudi[2], S. Joyson Abraham[3]*, G. Gifta Jerith[4], J. Ebenezer Samuel Daniel[5]

1,2 Dept. of Aeronautical Engineering, Malla Reddy College of Engineering & Technology, Hyderabad, India.

3* Dept. of Mechanical Engineering, Malla Reddy College of Engineering & Technology, Hyderabad, India.

4 Dept. of AI & ML, School of Engineering, Malla Reddy University, Hyderabad, Telangana, India.

5 Dept. of Mechanical Engineering, Jayaraj Annapackiam CSI College of Engineering, Tamil Nadu, India.

Abstract - Wingtip vortices generated by finite wings increase induced drag and degrade aerodynamic efficiency. This study compares a baseline wing with four wingtip configurations: a raked wingtip, wingtip fence, blended winglet, and split scimitar winglet. Parametric three-dimensional models were evaluated under a common low-speed cruise condition using steady Reynolds-averaged Navier-Stokes simulations and the finite-volume method. The comparison considers pressure-coefficient distributions, velocity streamlines, Mach-number contours, turbulent kinetic energy, and downstream vortex development. Relative to the baseline, each wingtip device weakened the concentrated tip vortex and improved pressure recovery, although the degree of improvement depended on geometry. The raked wingtip and wingtip fence produced moderate improvements, whereas the blended winglet generated a smoother wing-winglet flow transition and a more diffuse wake. Within the conditions and qualitative indicators examined, the split scimitar configuration produced the weakest vortex signature and the most uniform downstream flow field. The results demonstrate the importance of wingtip geometry in controlling three-dimensional wake development and provide a basis for subsequent force-based validation, mesh-sensitivity assessment, and experimental investigation.

Keywords: computational fluid dynamics; induced drag; wingtip vortex; blended winglet; split scimitar winglet; wake development.

I. 1. Introduction

The aviation industry has experienced unprecedented growth over the past several decades owing to the continuous increase in global air transportation, rapid technological advancements, and expanding commercial operations. This remarkable growth has substantially increased fuel consumption, operating costs, and greenhouse gas emissions, thereby intensifying the demand for environmentally sustainable and energy-efficient aircraft technologies. Consequently, improving aerodynamic performance has become one of the principal objectives in modern aircraft design, as even marginal reductions in aerodynamic drag can produce considerable savings in fuel consumption, enhance flight range, reduce operational costs, and minimize carbon emissions throughout an aircraft's service life [1–3]. Among the various aerodynamic drag components acting on an aircraft, induced drag represents one of the most significant contributors during cruise conditions, particularly for subsonic and transonic transport aircraft. Induced drag originates from the finite span of the wing and is directly associated with the generation of wingtip vortices. During flight, the pressure difference between the lower-pressure surface and the upper suction surface causes airflow to migrate around the wingtip, forming a pair of counter-rotating vortices that persist downstream of the aircraft. These vortices represent a continuous loss of aerodynamic energy, reducing lift efficiency while simultaneously increasing drag and fuel consumption. Furthermore, wingtip vortices generate wake turbulence that adversely affects aircraft stability, structural loading, airport traffic separation, and overall flight safety. Consequently, reducing induced drag through effective wingtip flow control has become a major research priority in contemporary aerospace engineering [2–5].

To improve aerodynamic efficiency, numerous wingtip devices have been developed over the past five decades. Among these technologies, winglets have emerged as one of the most successful passive flow-control devices employed in modern commercial aircraft. Unlike conventional wing extensions, winglets modify the three-dimensional airflow near the wingtip by reducing pressure equalization between the pressure and suction surfaces. This mechanism weakens the strength of the trailing vortex, redistributes spanwise lift more efficiently, and reduces the aerodynamic energy dissipated within the wake. The resulting improvement in the lift-to-drag ratio contributes directly to lower fuel consumption, reduced operating costs, increased flight range, and decreased environmental impact. Consequently, advanced winglet configurations have become standard aerodynamic features on numerous commercial aircraft developed by Boeing, Airbus, and other major aerospace manufacturers [4–7]. The modern winglet concept was pioneered by **Richard T. Whitcomb** of the National Aeronautics and Space Administration (NASA), who demonstrated that carefully designed wingtip devices could significantly reduce induced drag without requiring a substantial increase in wingspan [4]. Whitcomb's pioneering experimental investigations established the aerodynamic principles governing winglet performance and demonstrated measurable improvements in cruise efficiency and fuel economy. His research fundamentally changed aircraft wing design and laid the foundation for the development of advanced wingtip devices used in modern aviation. The successful implementation of Whitcomb's concept subsequently encouraged extensive experimental, analytical, and numerical investigations aimed at improving wingtip aerodynamic performance under a wide range of operating conditions [4,5].

Following Whitcomb's pioneering work, Kroo expanded the theoretical understanding of induced drag reduction by investigating optimum spanwise lift distribution and wingtip geometry optimization [5]. His studies demonstrated that the aerodynamic effectiveness of a wingtip device depends not only on increasing the effective aspect ratio of the wing but also on minimizing aerodynamic interference while satisfying structural and manufacturing constraints. These theoretical developments provided the scientific basis for designing advanced winglet configurations capable of improving aerodynamic efficiency without imposing excessive structural penalties. Consequently, researchers proposed several innovative wingtip concepts, including raked wingtips, wingtip fences, blended winglets, split scimitar winglets, spiroid winglets, and morphing winglets, each employing different aerodynamic mechanisms to suppress vortex formation and reduce induced drag [5–9]. The continuous evolution of computational techniques has further accelerated the development of winglet technology. In particular, Computational Fluid Dynamics (CFD) has become an indispensable tool for investigating complex three-dimensional flow phenomena associated with aircraft wings and wingtip devices. Modern CFD techniques enable detailed visualization of pressure distributions, velocity streamlines, vortex structures, Mach number variations, turbulent kinetic energy, and wake development, providing comprehensive insight into aerodynamic behaviour that is often difficult to obtain exclusively through wind tunnel experiments. Furthermore, advances in numerical algorithms, turbulence modelling, and high-performance computing have significantly improved the reliability and accuracy of CFD simulations, making numerical analysis an essential component of aircraft aerodynamic design and optimization [10–13].

The adoption of Reynolds-Averaged Navier–Stokes (RANS)-based numerical methods, together with appropriate turbulence closures, has enabled accurate prediction of flow separation, adverse pressure gradients, and wingtip vortex evolution under realistic flight conditions [11–14]. These developments have substantially reduced the time and cost associated with aerodynamic design optimization while enabling researchers to evaluate multiple winglet configurations before prototype manufacturing. Consequently, CFD has become one of the most widely adopted methodologies for analysing the aerodynamic characteristics of modern aircraft wings, allowing systematic comparison of alternative wingtip geometries based on pressure recovery, vortex suppression, wake stability, and overall aerodynamic efficiency [12–15]. Recent investigations have demonstrated that modern winglet geometries provide substantial aerodynamic improvements compared with conventional vertical winglets. Blended winglets have been reported to improve lift distribution by eliminating abrupt geometric discontinuities at the wing–winglet junction, thereby reducing interference drag and weakening wingtip vortices [16–18]. Similarly, wingtip fences have been shown to restrict spanwise airflow through the incorporation of upper and lower vertical lifting surfaces, resulting in moderate reductions in induced drag while maintaining structural simplicity [17,19]. Raked wingtips improve aerodynamic performance primarily by increasing the effective span of the wing, thereby reducing vortex strength through a more favourable lift distribution [18–20]. More recently, split scimitar winglets have attracted considerable attention because of their ability to modify the three-dimensional vortex structure through the incorporation of an additional ventral strake, leading to improved pressure recovery, enhanced wake stability, and superior fuel efficiency compared with earlier winglet designs [20–23].

2. WINGLET DESIGN CONCEPTS AND AERODYNAMIC CHARACTERISTICS

2.1 Raked Wingtip

The raked wingtip is a swept extension of the main wing that increases the effective wingspan without incorporating a vertically oriented winglet. Unlike conventional winglets, the raked wingtip remains nearly coplanar with the wing and extends outward with a larger leading-edge sweep angle. This configuration enhances the span efficiency factor by producing a lift distribution that more closely approaches the ideal elliptical distribution, thereby reducing induced drag and improving cruise performance.

From an aerodynamic perspective, the extended wingtip delays the roll-up of the trailing vortex and reduces its overall strength by distributing the aerodynamic loading over a larger effective span. The gradual reduction in local lift near the wingtip minimizes pressure gradients and contributes to smoother airflow around the wingtip region. These characteristics make the raked wingtip particularly suitable for long-range transport aircraft operating predominantly under cruise conditions, where improvements in fuel efficiency and aerodynamic performance are highly desirable. However, the increased wingspan also leads to higher wing-root bending moments, which may require additional structural reinforcement and increase the overall structural weight of the aircraft. Furthermore, since the raked wingtip primarily improves span efficiency rather than actively diffusing the wingtip vortex, its effectiveness in reducing induced drag and suppressing wake vortices is generally lower than that of advanced blended or split scimitar winglets.

Figure 1 illustrates the five wingtip configurations considered in the present investigation, including the baseline wing, raked wingtip, wingtip fence, blended winglet, and split scimitar winglet. Each configuration modifies the three-dimensional airflow near the wingtip through a distinct aerodynamic mechanism, thereby influencing induced drag, wingtip-vortex development, and wake behaviour. The geometrical differences among these configurations form the basis for the comparative computational analysis presented in this study.

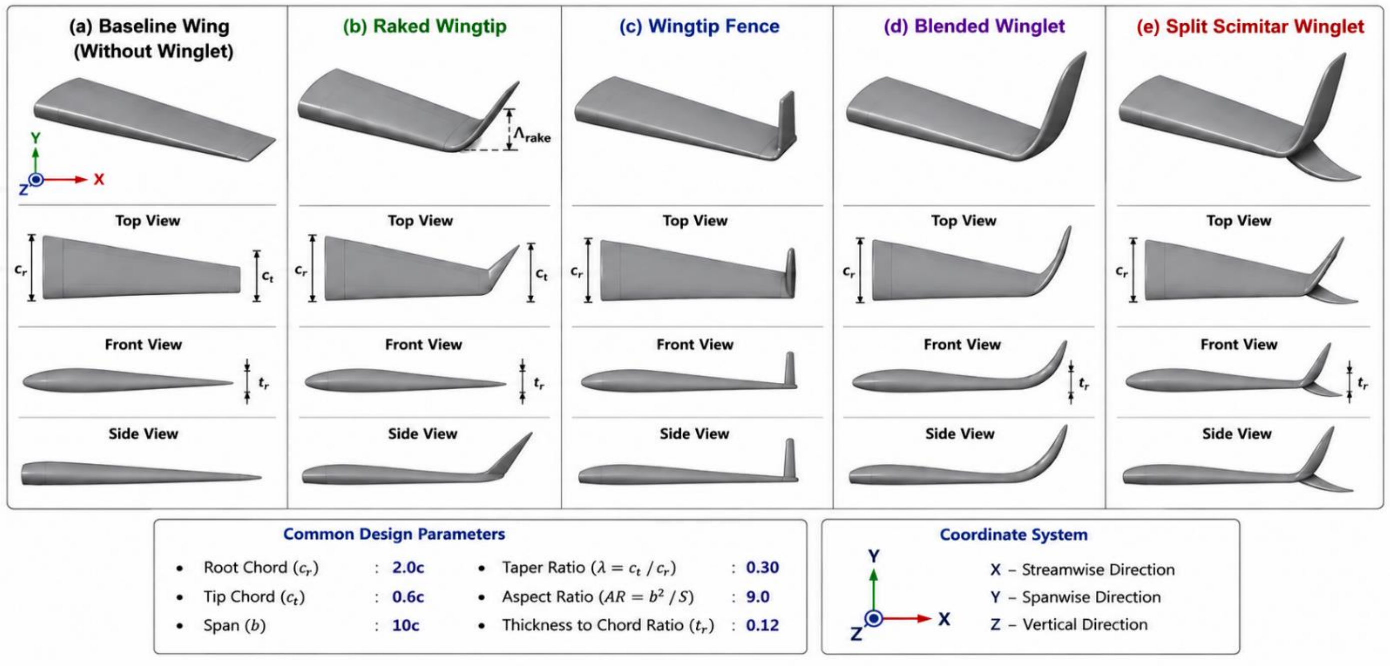

Figure 1. Schematic representation of the baseline wing and winglet configurations considered in the present study: (a) Baseline wing, (b) Raked wingtip, (c) Wingtip fence, (d) Blended winglet, and (e) Split scimitar winglet.

2.2 Wingtip Fence

The wingtip fence consists of two relatively small aerodynamic surfaces extending upward and downward from the wingtip. Unlike conventional winglets that project primarily upward, the wingtip fence simultaneously restricts airflow migration above and below the wing, thereby reducing the pressure equalization responsible for wingtip vortex formation.
The upper and lower fence surfaces partially block the spanwise airflow, decreasing the intensity of the wingtip vortex and improving the local pressure distribution around the wingtip. Owing to its relatively simple construction, low structural weight, and ease of installation, the wingtip fence has been widely adopted on several commercial aircraft, particularly within the Airbus A320 family. This configuration provides moderate reductions in induced drag, improves fuel economy, and enhances overall flight stability while maintaining comparatively low manufacturing and maintenance costs. Nevertheless, the relatively limited aerodynamic surface area restricts its ability to significantly modify the vortex structure under high-lift and transonic operating conditions. Consequently, its aerodynamic efficiency and lift-to-drag ratio improvements are generally lower than those achieved by blended or split scimitar winglets.

2.3 Blended Winglet

The blended winglet represents one of the most successful wingtip technologies implemented in modern commercial aviation. Unlike conventional winglets connected through a sharp junction, the blended winglet incorporates a continuously curved transition between the main wing and the winglet. This smooth blending minimizes interference drag and flow separation near the wing–winglet junction while simultaneously increasing the effective aerodynamic span.
The aerodynamic principle of the blended winglet is based on redirecting the pressure-driven spanwise airflow into a controlled upward vortex structure. This redistribution weakens the primary trailing vortex, reduces induced drag, and significantly improves the lift-to-drag ratio. The smooth curvature also distributes aerodynamic loads more uniformly, reducing local stress concentrations and enhancing the structural integrity of the wing–winglet junction. Consequently, blended winglets have demonstrated substantial reductions in fuel consumption, improved climb performance, and increased operational range, making them one of the most widely adopted wingtip devices in modern commercial aviation. However, their smoothly curved geometry requires more sophisticated manufacturing techniques than simpler wingtip devices such as wingtip fences, leading to increased fabrication costs and slightly higher structural weight.

2.4 Split Scimitar Winglet

The split scimitar winglet represents an advanced evolution of the conventional blended winglet. This configuration combines an upward blended winglet with a downward curved ventral strake, producing a characteristic scimitar-shaped geometry. The additional lower aerodynamic surface modifies the three-dimensional flow field by dividing the primary wingtip vortex into two weaker counter-rotating vortices, thereby significantly reducing vortex intensity and improving aerodynamic efficiency.
The interaction between the upper and lower winglet surfaces decreases induced drag and reduces turbulent kinetic energy within the aircraft wake. The redistribution of aerodynamic loading also minimizes unsteady pressure fluctuations acting on the wingtip, resulting in lower unsteady aerodynamic loading and improved wake stability. Owing to these aerodynamic characteristics, the split scimitar winglet provides the greatest improvement in fuel efficiency, aircraft range, and overall aerodynamic performance among the winglet configurations investigated in this study. Nevertheless, its complex three-dimensional geometry increases manufacturing complexity, installation cost, and structural weight compared with conventional winglet designs. Despite these limitations, the significant aerodynamic benefits generally outweigh the additional manufacturing requirements, making the split scimitar winglet one of the most effective wingtip technologies currently employed in modern commercial aircraft.

2.5 Comparative Evaluation of Winglet Configurations

The aerodynamic performance of a wingtip device is governed primarily by its capability to modify the three-dimensional flow field near the wingtip, thereby reducing induced drag and improving the overall aerodynamic efficiency of the aircraft. Although all the investigated winglet configurations are designed to suppress wingtip vortices, each employs a different aerodynamic mechanism and consequently exhibits distinct advantages and limitations. A systematic comparison of these configurations is therefore essential for understanding their influence on pressure recovery, vortex attenuation, wake stability, and aerodynamic performance.

The raked wingtip enhances aerodynamic efficiency by extending the effective wingspan, thereby producing a more favourable spanwise lift distribution and reducing induced drag during cruise flight. This configuration is particularly effective for long-range transport aircraft because it improves span efficiency while maintaining a relatively simple aerodynamic profile. However, the increased wingspan produces higher wing-root bending moments, which may require additional structural reinforcement and increase the structural weight of the aircraft.

The wingtip fence modifies the aerodynamic flow by restricting spanwise airflow using vertically oriented upper and lower lifting surfaces. This configuration reduces the pressure equalization responsible for wingtip vortex formation and provides moderate improvements in aerodynamic efficiency while maintaining low structural complexity. Owing to its lightweight construction and ease of integration, the wingtip fence has been widely adopted on several commercial aircraft. Nevertheless, its comparatively small aerodynamic surface limits its effectiveness under high-lift and transonic operating conditions.

The blended winglet provides a more advanced aerodynamic solution by incorporating a smooth transition between the main wing and the winglet. The continuous curvature minimizes interference drag, improves pressure recovery, and promotes gradual vortex diffusion. Consequently, blended winglets achieve significant improvements in lift-to-drag ratio, fuel efficiency, and cruise performance. Their primary limitation is the increased manufacturing complexity associated with the smoothly blended geometry.

Among the investigated configurations, the split scimitar winglet represents the most advanced aerodynamic concept. The incorporation of a downward-curved ventral strake beneath the blended winglet modifies the three-dimensional flow structure by dividing the primary wingtip vortex into weaker counter-rotating vortices. This mechanism provides superior vortex suppression, improved wake stability, reduced compressibility effects, and enhanced aerodynamic efficiency compared with the other investigated configurations. Although its complex geometry results in higher manufacturing and installation costs, the aerodynamic benefits generally outweigh these additional engineering requirements.

Table 1 presents a comparative summary of the aerodynamic principles, principal advantages, engineering limitations, and representative aircraft applications of the investigated winglet configurations. The comparison illustrates the progressive evolution of wingtip technology from the conventional baseline wing to modern split scimitar winglets and highlights the engineering considerations associated with each design. This comparative evaluation establishes the foundation for the CAD modelling and Computational Fluid Dynamics (CFD) analyses presented in the subsequent sections.

Table 1. Comparative characteristics of the investigated winglet configurations.

Winglet Configuration	Aerodynamic Principle	Major Advantages	Engineering Limitations	Representative Aircraft
Baseline Wing	Conventional finite-span wing without a wingtip device	Simple geometry, low manufacturing complexity	Strong wingtip vortices, high induced drag, greater wake turbulence	Conventional transport aircraft
Raked Wingtip	Extends the effective wingspan to improve span efficiency and lift distribution	Reduced induced drag, improved cruise efficiency, enhanced lift distribution	Increased wing-root bending moment and structural weight	Boeing 777, Boeing 787
Wingtip Fence	Restricts spanwise airflow using upper and lower vertical aerodynamic surfaces	Moderate drag reduction, lightweight design, simple installation	Limited vortex suppression under transonic conditions	Airbus A320 family
Blended Winglet	Smooth wing–winglet transition minimizes interference drag and promotes vortex diffusion	Improved lift-to-drag ratio, lower fuel consumption, enhanced climb performance	Higher manufacturing complexity and fabrication cost	Boeing 737 Next Generation, Boeing 757
Split Scimitar Winglet	Additional ventral strake divides the primary vortex into weaker counter-rotating vortices	Superior vortex suppression, excellent pressure recovery, improved wake stability, highest aerodynamic efficiency	Increased geometric complexity, structural weight, and installation cost	Boeing 737 NG (retrofit), Boeing 737 MAX

3. CAD Modelling of Winglet Configurations

The three-dimensional geometrical models of the aircraft wing and the various winglet configurations were developed using a computer-aided design (CAD) environment to establish accurate computational models for the subsequent aerodynamic analyses. The CAD models were generated by maintaining a common baseline wing geometry while modifying only the wingtip region to accommodate different winglet configurations. This approach ensured that the aerodynamic performance of each configuration could be evaluated under identical geometric conditions, thereby providing a consistent basis for comparison.

The baseline wing was initially modelled as a tapered finite wing with smooth aerodynamic surfaces. The wing planform was defined using the prescribed span, root chord, tip chord, taper ratio, and sweep angle. A suitable airfoil profile was employed along the spanwise direction, and lofting techniques were used to generate a continuous three-dimensional wing surface. The resulting geometry accurately represents the external aerodynamic shape required for computational fluid dynamics (CFD) analysis.

Following the construction of the baseline model, four different wingtip configurations were developed by modifying only the outermost section of the wing. The raked wingtip was created by extending the wing in the spanwise direction with an increased leading-edge sweep, thereby improving the effective aspect ratio while maintaining a continuous wing surface. The wingtip fence configuration incorporated vertically oriented upper and lower aerodynamic surfaces positioned at the wingtip to restrict spanwise airflow and reduce the intensity of the trailing vortex. The blended winglet was designed using a smooth fillet transition between the wing and the winglet, minimizing interference drag and ensuring a gradual redistribution of aerodynamic loading. Finally, the split scimitar winglet was generated by incorporating an additional downward-curved ventral strake beneath the blended winglet, producing a more complex three-dimensional geometry intended to further weaken the wingtip vortex and enhance aerodynamic efficiency.

To ensure a fair comparison among all configurations, identical wing dimensions, airfoil profile, and primary geometric parameters were maintained throughout the modelling process, while only the wingtip geometry was varied. This modelling strategy isolates the influence of winglet design on aerodynamic behaviour and eliminates the effects of other geometric variables. Furthermore, all models were constructed as watertight solid bodies with smooth surface continuity to facilitate high-quality mesh generation and numerical convergence during CFD simulations.

The completed CAD models of the baseline wing and the four winglet configurations are presented in Figure 2. The figure illustrates the isometric, top, front, and side views of each configuration, highlighting the principal geometric differences between the raked wingtip, wingtip fence, blended winglet, and split scimitar winglet. These CAD models formed the basis for the computational domain generation, mesh development, and aerodynamic simulations performed in the present investigation.

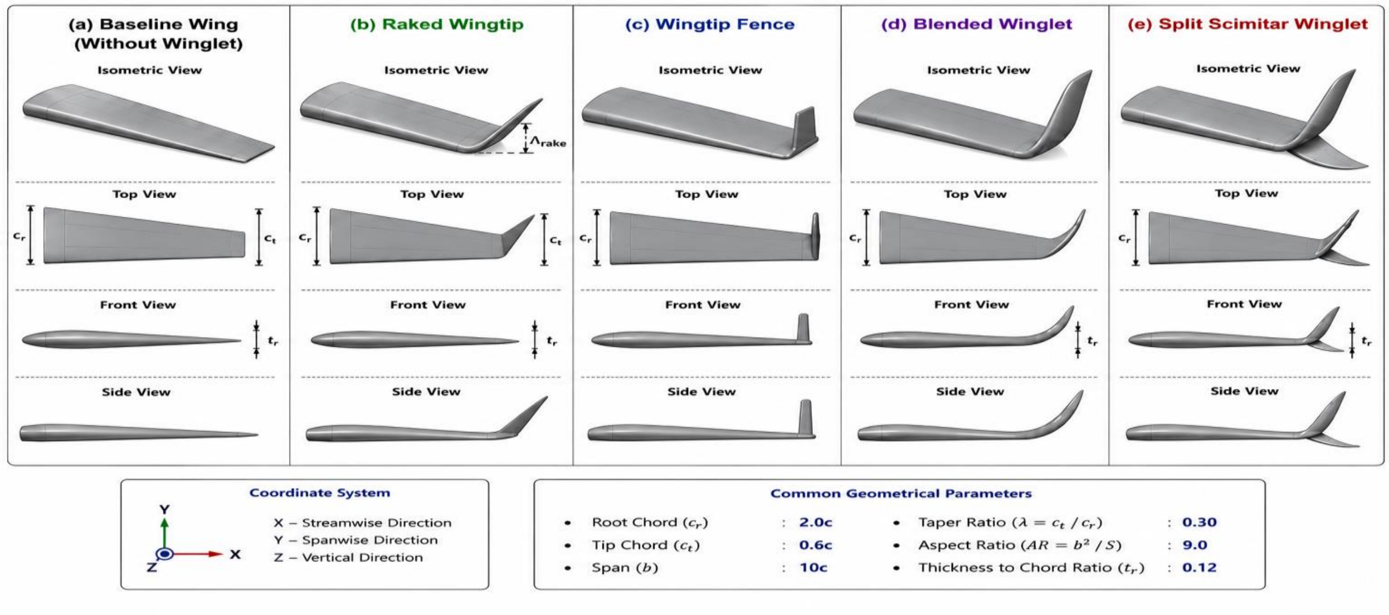

Figure 2. Three-dimensional CAD models of the baseline wing and the investigated winglet configurations used for the computational aerodynamic analysis.

4. Computational Fluid Dynamics Methodology

4.1 Computational Domain and Boundary Conditions

The aerodynamic characteristics of the baseline wing and four winglet configurations were investigated using three-dimensional Computational Fluid Dynamics (CFD) simulations. The numerical analysis was performed under steady-state conditions by solving the Reynolds–Averaged Navier–Stokes (RANS) equations using the finite volume method (FVM). The CFD methodology was adopted to predict the aerodynamic flow behaviour around the aircraft wing and evaluate the influence of different winglet geometries on pressure distribution, induced drag, wingtip vortex formation, and wake characteristics.

A rectangular domain measuring 20c in the streamwise direction and 10c in both the vertical and spanwise directions was used, where c denotes the root chord. The inlet was positioned 4c upstream of the leading edge and the outlet 15c downstream of the trailing edge. These extents reduced blockage and allowed the wake to develop before reaching the outlet.

A uniform free-stream velocity of 78.5 m/s (Mach 0.23) was imposed at the inlet at an angle of attack of 2°, and a gauge pressure of 0 Pa was specified at the outlet. The upper, lower, and lateral far-field boundaries were treated as symmetry boundaries. All wing and winglet surfaces were stationary no-slip walls. The X-, Y-, and Z-axes denote the streamwise, vertical, and spanwise directions, respectively.

The same computational domain and boundary conditions were maintained for all wing configurations to ensure a consistent comparison of their aerodynamic performance.

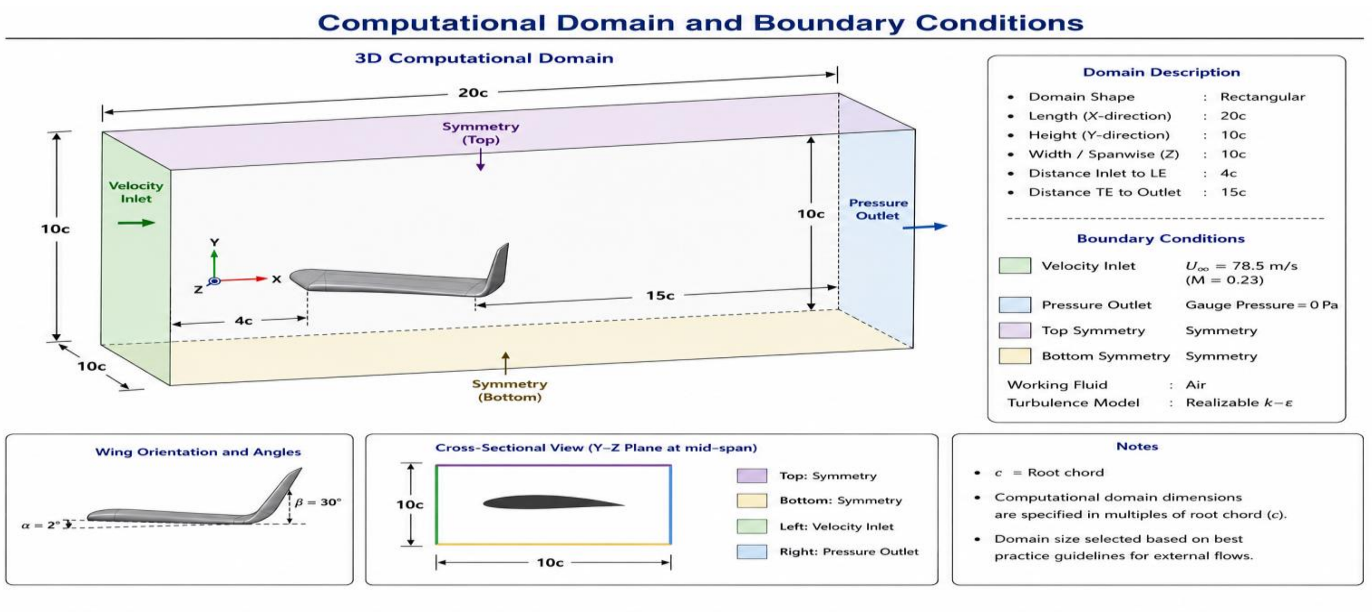

Figure 3. Computational domain and boundary conditions used for the numerical simulation.

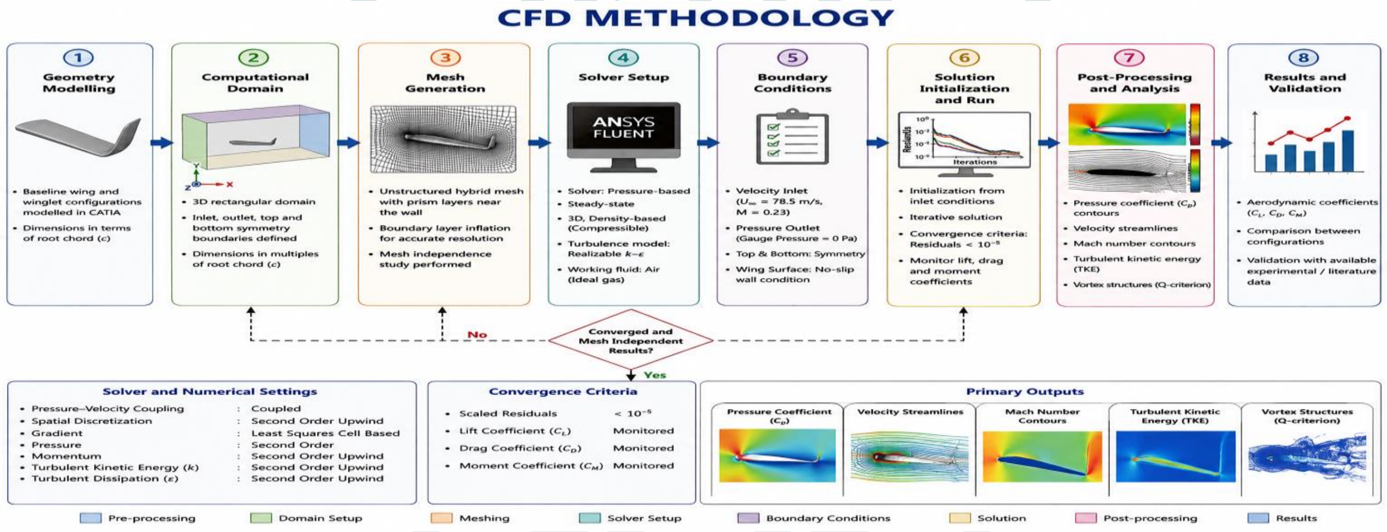

Figure 4. Workflow of the CFD methodology adopted for aerodynamic analysis of baseline and winglet configurations.

The overall methodology adopted in this study is illustrated in Figure 4. The workflow begins with the creation of the baseline wing and four winglet configurations, followed by CAD model development, computational domain generation, mesh generation, and mesh quality verification. Subsequently, appropriate boundary conditions and numerical models are applied for CFD simulations. Finally, the aerodynamic performance is evaluated through post-processing and comparative analysis to identify the optimal winglet configuration.

Table 2. CFD Simulation Parameters.

Parameter	Specification	Purpose
CFD Software	ANSYS Fluent	CFD solver used for aerodynamic simulations
Solver Type	Pressure-Based Solver	Suitable for incompressible and low-speed compressible flows
Analysis Type	Steady-State	Computes the converged steady aerodynamic flow field
Governing Equations	Reynolds–Averaged Navier–Stokes (RANS) Equations	Governs the conservation of mass and momentum
Numerical Method	Finite Volume Method (FVM)	Spatial discretization of governing equations
Turbulence Model	Realizable k–ε model	Turbulent external-flow closure
Working Fluid	Air	Fluid medium used in the simulation
Flow Regime	Turbulent	Represents realistic external aerodynamic flow
Inlet Boundary Condition	Velocity inlet: 78.5 m/s (M = 0.23)	Specifies incoming free-stream velocity

Parameter	Specification	Purpose
Outlet Boundary Condition	Pressure Outlet	Allows smooth exit of the airflow
Side Boundary Condition	Symmetry	Simulates an unconfined external flow domain
Wall Boundary Condition	No-Slip Wall	Enforces zero velocity at solid surfaces
Mesh Type	Unstructured Tetrahedral Mesh	Suitable for complex three-dimensional geometries
Near-Wall Treatment	20 prism inflation layers; growth rate 1.2	Resolves near-wall boundary-layer gradients
Pressure–Velocity Coupling	SIMPLE Algorithm	Couples pressure and velocity fields
Momentum Discretization	Second-Order Upwind Scheme	Improves numerical accuracy
Turbulence Discretization	Second-Order Upwind Scheme	Reduces numerical diffusion
Pressure Interpolation	Second-Order	Enhances pressure prediction accuracy
Solution Initialization	Standard Initialization	Provides initial conditions for the solver
Convergence Criterion	Residuals < 10^{-6}	Ensures numerical convergence

The numerical simulations were carried out using the parameters listed in Table 2. Identical solver settings, boundary conditions, and numerical schemes were employed across all winglet configurations to ensure that the observed aerodynamic differences were attributable solely to changes in winglet geometry.

4.2 Mesh Generation

The computational domain was discretized with a hybrid finite-volume mesh containing approximately 12.44 million elements and 2.26 million nodes. Twenty prism inflation layers were applied adjacent to the wing surface with a growth rate of 1.2, while unstructured tetrahedral elements filled the core region. Local refinement was concentrated near the leading edge, trailing edge, wingtip, winglet junction, and downstream wake. Inflation layers were generated adjacent to all solid surfaces to improve the resolution of the near-wall boundary layer. The inflation mesh provided smooth growth of the boundary-layer cells away from the wall, thereby enhancing the prediction of wall shear stress and flow separation.
Mesh quality was assessed using skewness and orthogonality. The reported average skewness was 0.23, the maximum skewness was 0.74, and the average orthogonality was 69.3°. These values were within the limits adopted for the present simulations. A formal grid-independence study should nevertheless be reported before the quantitative force coefficients are used for design decisions.

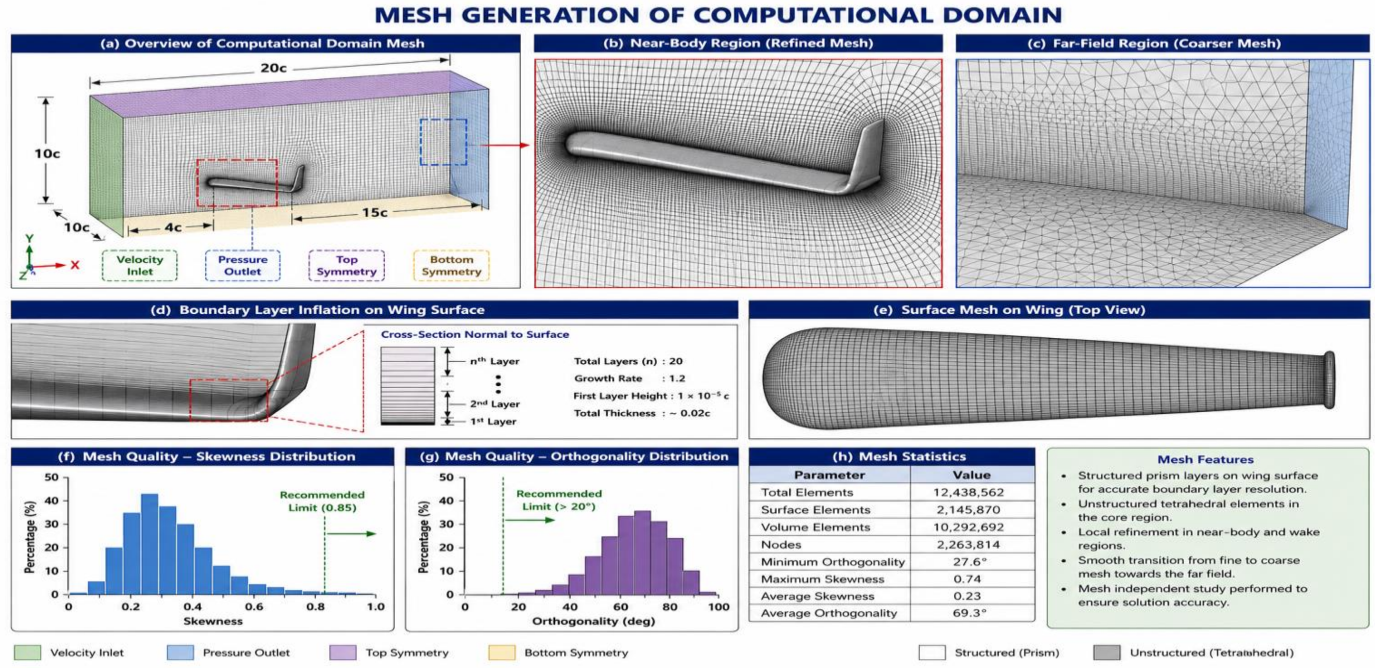

Figure 5. Unstructured computational mesh showing local refinement around the wingtip and inflation layers adjacent to the wing surface.

4.3 Numerical Solution Procedure

The governing continuity and momentum equations were solved using a pressure-based solver with the SIMPLE algorithm for pressure–velocity coupling. Second-order upwind discretization schemes were adopted for the momentum and turbulence equations to improve numerical accuracy and reduce discretization errors.
The realizable k–ε turbulence model was selected because of its ability to accurately predict adverse pressure gradients, boundary-layer development, flow separation, and wingtip vortex behaviour. This model combines the advantages of the standard k–ω model in the near-wall region with the robustness of the k–ε model in the free stream, making it suitable for external aerodynamic simulations of aircraft wings.
The solution was considered converged when the normalized residuals of the continuity, momentum, and turbulence equations fell below 10^{-6} and the monitored aerodynamic quantities no longer exhibited systematic drift. Identical convergence criteria were applied to all five configurations.

4.4 Aerodynamic Performance Evaluation

The aerodynamic performance of the baseline wing and the four winglet configurations was evaluated using several flow-field parameters obtained from the CFD simulations. These included pressure coefficient distribution, velocity streamlines, wingtip vortex structure, Mach number contours, turbulent kinetic energy (TKE), wake development, and overall aerodynamic flow behaviour. Comparative analysis of these parameters enabled the assessment of the effectiveness of each winglet configuration in suppressing wingtip vortices, improving pressure recovery, and enhancing aerodynamic efficiency. The results obtained from the CFD simulations are presented and discussed in the subsequent section.

5. RESULTS AND DISCUSSION

5.1 Pressure Coefficient Distribution

The pressure-coefficient contours presented in Figure 6 demonstrate the influence of winglet geometry on the aerodynamic pressure field developed over the wing surface. A comparison of the five configurations reveals substantial differences in the pressure recovery characteristics, indicating that the geometry of the wingtip plays a dominant role in governing induced drag and vortex formation.

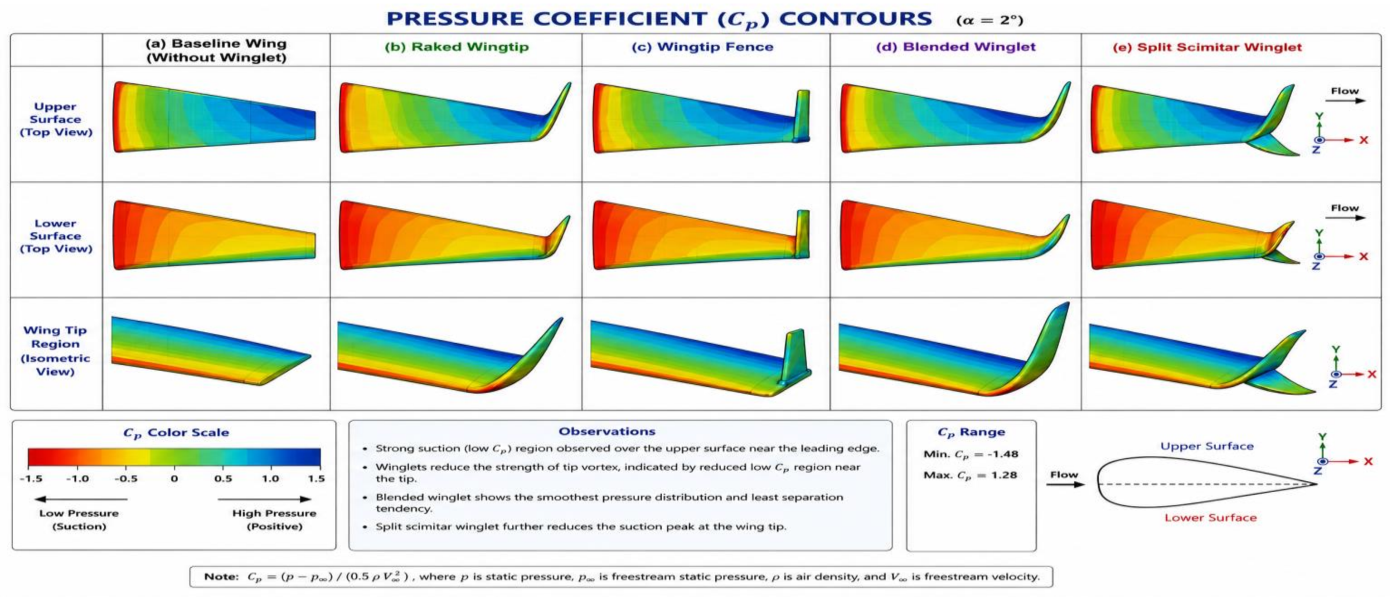

Figure 6. Pressure coefficient contours illustrating the influence of different winglet configurations on the aerodynamic pressure distribution.

As illustrated in Figure 6(a), the baseline wing exhibits a pronounced low-pressure region over the upper wing surface near the tip, accompanied by a corresponding high-pressure region beneath the wing. This large pressure differential promotes intense spanwise flow around the wingtip, leading to the formation of a concentrated trailing vortex. The steep pressure gradient observed near the tip indicates significant aerodynamic energy loss through induced drag and contributes to the development of an energetic wake.

The pressure contours obtained for the raked wingtip, shown in Figure 6(b), indicate a noticeable improvement in pressure distribution compared with the baseline configuration. The extension of the wingtip increases the effective span and produces a more gradual reduction in pressure toward the wingtip region. Consequently, the spanwise pressure gradient decreases, delaying vortex roll-up and reducing induced drag. Nevertheless, localized pressure concentrations remain visible near the outer section of the wing, indicating that vortex suppression is only partially achieved.

The wingtip fence configuration illustrated in Figure 6(c) exhibits a more uniform pressure field than both the baseline and raked wingtip configurations. The upper and lower fence surfaces restrict spanwise airflow and reduce pressure equalization between the upper and lower wing surfaces. As a result, the adverse pressure gradient near the wingtip decreases, producing a weaker trailing vortex. However, because the aerodynamic surface area of the fence is relatively limited, the improvement in pressure recovery remains moderate.

A further enhancement is observed in the blended winglet configuration presented in Figure 6(d). The smoothly curved transition between the wing and the winglet redistributes the pressure loading more uniformly along the wingtip, eliminating abrupt pressure variations that typically occur near conventional wingtip junctions. The gradual pressure recovery suggests a significant reduction in induced drag and demonstrates the effectiveness of the blended geometry in improving aerodynamic efficiency.

Among all configurations, the split scimitar winglet shown in Figure 6(e) exhibits the most uniform pressure distribution across the wingtip region. The additional ventral strake modifies the three-dimensional pressure field by redirecting part of the spanwise flow beneath the wing while simultaneously weakening the primary vortex above the wing. The resulting pressure contours display smoother gradients and reduced localized pressure concentrations, indicating more effective vortex suppression and improved aerodynamic loading. These characteristics suggest that the split scimitar winglet provides the highest aerodynamic efficiency among the investigated configurations.

The comparative analysis presented in Figure 6 clearly demonstrates that improvements in pressure recovery become progressively more significant from the baseline wing to the split scimitar winglet. The ability of advanced winglet geometries to redistribute aerodynamic loading and reduce spanwise pressure gradients directly contributes to lower induced drag, improved lift distribution, and enhanced cruise performance. Similar trends have been reported in previous numerical investigations of advanced wingtip devices, confirming the effectiveness of blended and split scimitar winglets in improving aerodynamic efficiency.

5.2 Velocity Streamlines and Wingtip Vortex Structure

The velocity streamlines and wingtip vortex structures obtained from the computational analysis are presented in Figure 7. The streamline visualization provides valuable insight into the development of three-dimensional airflow around the wingtip and illustrates the influence of different winglet geometries on vortex formation, wake evolution, and aerodynamic efficiency. The generation of trailing vortices is a direct consequence of the pressure difference between the upper and lower wing surfaces, resulting in spanwise airflow that rolls into concentrated vortical structures downstream of the wing. These vortices represent aerodynamic energy losses that contribute significantly to induced drag and wake turbulence.

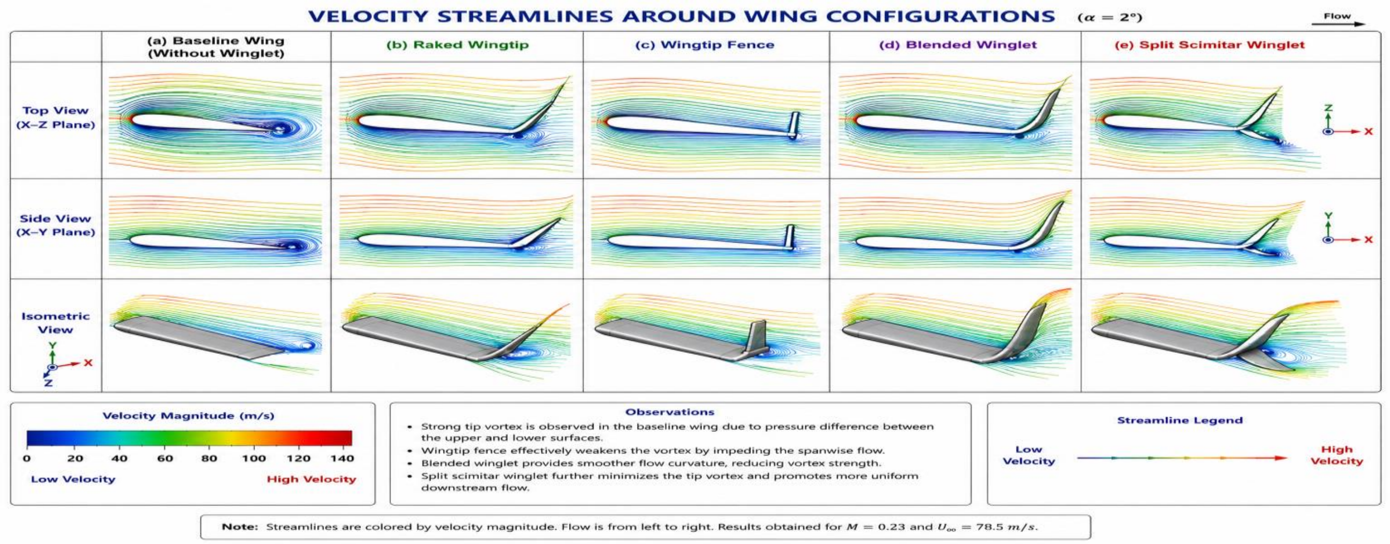

Figure 7. Velocity streamlines and wingtip vortex structures for the baseline wing and the investigated winglet configurations.

As illustrated in Figure 7(a), the baseline wing produces a highly concentrated wingtip vortex immediately downstream of the trailing edge. The velocity streamlines exhibit strong spanwise flow from the pressure side to the suction side of the wing, forming a compact vortex core that persists over a considerable downstream distance. The high velocity gradients surrounding the vortex indicate significant rotational kinetic energy within the wake, leading to increased induced drag and stronger wake turbulence. The concentrated vortex also generates unsteady aerodynamic loading near the wingtip, which may increase unsteady aerodynamic loading and reduce aerodynamic efficiency.

The streamline distribution corresponding to the raked wingtip, shown in Figure 7(b), demonstrates a noticeable modification of the wake structure. The extended wingtip increases the effective wingspan, allowing the aerodynamic loading to be distributed over a larger lifting surface. Consequently, the velocity streamlines remain attached over a longer spanwise distance before rolling into the trailing vortex. The resulting vortex exhibits a larger diameter and lower rotational intensity compared with the baseline configuration, indicating partial suppression of vortex strength and a reduction in induced drag. However, the primary vortex remains clearly identifiable, suggesting that the aerodynamic improvement is primarily associated with enhanced span efficiency rather than complete vortex diffusion.

The wingtip fence configuration presented in Figure 7(c) exhibits a different aerodynamic behaviour. The upper and lower fence surfaces restrict the spanwise migration of airflow, thereby reducing the interaction between the pressure and suction surfaces near the wingtip. As a result, the velocity streamlines display reduced curvature around the wingtip, and the wake develops more gradually than in the baseline case. The trailing vortex becomes less concentrated, indicating a reduction in vortex strength and wake turbulence. Nevertheless, the relatively limited aerodynamic surface area of the fence restricts its ability to fully redistribute the flow field, resulting in only moderate improvements in vortex suppression.

A more significant modification of the flow structure is observed for the blended winglet, illustrated in Figure 7(d). The smooth transition between the wing and the winglet redirects the spanwise airflow upward while maintaining attached flow around the wing–winglet junction. This gradual redirection of the flow weakens the primary trailing vortex and produces a more diffuse wake structure. The velocity streamlines remain smooth and continuous throughout the wingtip region, indicating reduced flow separation and improved aerodynamic stability. The diminished vortex intensity demonstrates that the blended winglet effectively converts part of the rotational energy associated with the trailing vortex into useful aerodynamic lift, thereby improving the lift-to-drag ratio and reducing induced drag.

Among all the investigated configurations, the split scimitar winglet, shown in Figure 7(e), exhibits the most favourable streamline characteristics. The addition of the downward-curved ventral strake modifies the three-dimensional flow field by dividing the primary wingtip vortex into two weaker counter-rotating vortices. This vortex-splitting mechanism significantly reduces the rotational energy contained within the wake and accelerates vortex dissipation downstream of the wing. The velocity streamlines appear more uniformly distributed around the wingtip, indicating improved flow stability and reduced aerodynamic energy loss. Furthermore, the weakened wake structure suggests lower wake turbulence and enhanced aerodynamic efficiency, making the split scimitar winglet the most effective configuration among those investigated.

A comparative examination of Figure 7(a–e) clearly demonstrates the progressive improvement in aerodynamic flow behaviour with increasing winglet complexity. The baseline wing generates the strongest trailing vortex, whereas the raked wingtip and wingtip fence provide moderate reductions in vortex intensity through span extension and spanwise flow restriction, respectively. The blended winglet further enhances aerodynamic performance by smoothly redirecting the airflow and promoting gradual vortex diffusion. The split scimitar winglet provides the highest level of vortex suppression by dividing the primary vortex into weaker counter-rotating structures, thereby minimizing induced drag and improving wake stability. These observations agree well with established aerodynamic theory, which indicates that effective wingtip devices reduce induced drag by weakening the pressure-driven vortex system rather than simply increasing the geometric wingspan.

The streamline analysis therefore confirms that the aerodynamic performance of modern winglet configurations is governed primarily by their ability to control three-dimensional flow development near the wingtip. By reducing vortex intensity, promoting smoother wake dissipation, and improving spanwise lift distribution, advanced winglet designs contribute directly to enhanced cruise efficiency, reduced fuel consumption, improved aircraft stability, and lower structural loading. Consequently, the split scimitar winglet represents the most aerodynamically efficient configuration investigated in the present study, followed by the blended winglet, raked wingtip, wingtip fence, and the baseline wing

5.3 Mach Number and Turbulent Kinetic Energy Distribution

The Mach number and turbulent kinetic energy (TKE) distributions obtained from the computational analysis are presented in Figure 8. These contours provide a comprehensive understanding of the influence of winglet geometry on compressible flow behaviour, local flow acceleration, wake turbulence, and aerodynamic energy dissipation. The Mach number contours identify regions of high local velocity where compressibility effects become significant, whereas the TKE contours illustrate the distribution of turbulent energy generated by vortex formation and wake development. Together, these flow-field characteristics provide valuable insight into the aerodynamic efficiency of each winglet configuration.

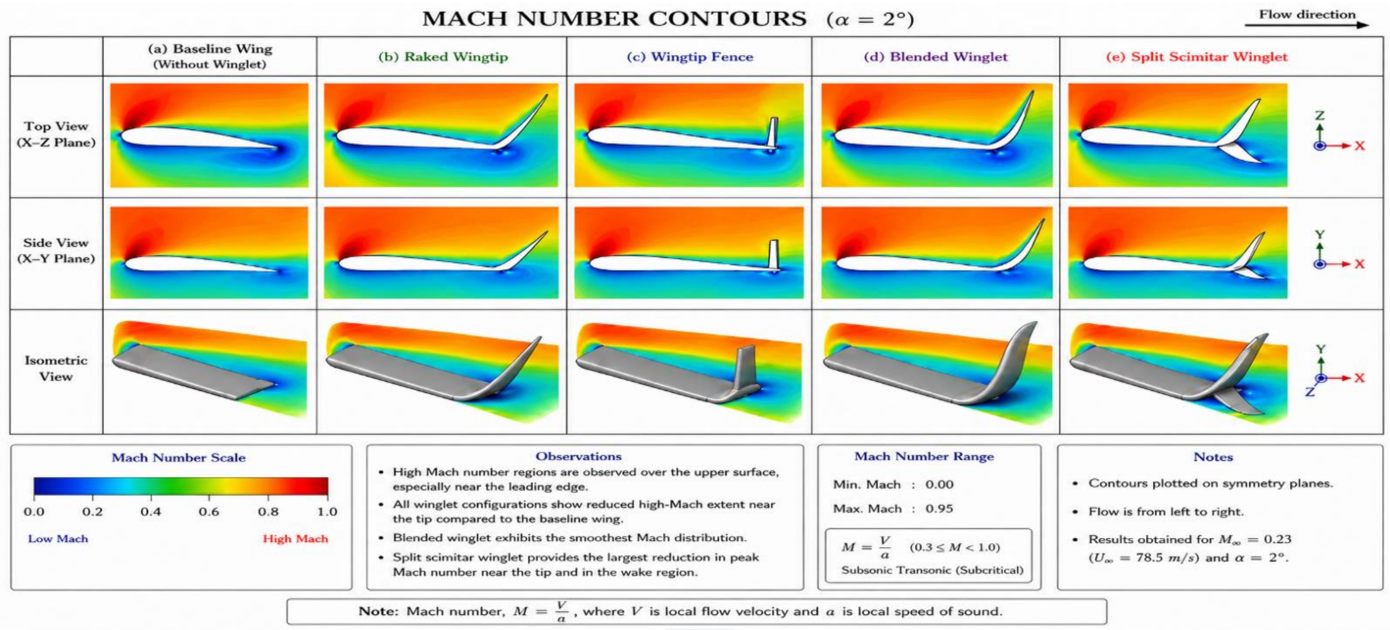

Figure 8. Mach number and turbulent kinetic energy contours comparing the aerodynamic performance of the investigated winglet configurations.

As illustrated in Figure 8(a), the baseline wing exhibits the largest region of elevated Mach number near the wingtip. The rapid acceleration of airflow over the upper wing surface results in the formation of a pronounced high-speed flow region accompanied by strong pressure gradients. This localized acceleration promotes the development of compressibility effects and increases the likelihood of compressibility-related formation under transonic operating conditions. The corresponding turbulent kinetic energy contours reveal an intense concentration of turbulence within the wake immediately downstream of the wingtip, indicating the presence of a highly energetic trailing vortex. The combined increase in local Mach number and turbulence intensity contributes to greater aerodynamic losses, higher induced drag, and reduced overall aerodynamic efficiency.
The raked wingtip configuration shown in Figure 8(b) exhibits a noticeable improvement in the flow-field characteristics compared with the baseline wing. The extended wingtip redistributes the aerodynamic loading over a larger effective span, resulting in a more gradual acceleration of the airflow near the wingtip. Consequently, the region of elevated Mach number becomes smaller and more uniformly distributed. The turbulent kinetic energy contours further indicate a reduction in wake turbulence, reflecting the delayed roll-up and weakened intensity of the trailing vortex. Although compressibility effects remain evident, the raked wingtip demonstrates a moderate improvement in aerodynamic performance through enhanced span efficiency and smoother wake development.
The Mach number contours corresponding to the wingtip fence, presented in Figure 8(c), demonstrate that restricting spanwise airflow modifies the local velocity field around the wingtip. The upper and lower fence surfaces reduce pressure equalization between the upper and lower wing surfaces, thereby decreasing local flow acceleration. As a result, the high-Mach-number region becomes less pronounced than that observed for the baseline wing. Similarly, the turbulent kinetic energy distribution indicates a reduction in vortex-induced turbulence, suggesting that the wingtip fence effectively suppresses part of the aerodynamic energy transferred into the wake. Nevertheless, the remaining turbulence concentration indicates that the fence primarily limits vortex formation rather than completely diffusing the wake structure.
A more substantial improvement is observed for the blended winglet configuration shown in Figure 8(d). The smoothly curved transition between the wing and the winglet promotes gradual pressure recovery and a more uniform redistribution of aerodynamic loading, resulting in smoother velocity gradients throughout the wingtip region. The Mach number contours indicate a noticeable reduction in the extent of high-speed flow, suggesting weaker compressibility effects and delayed compressibility-related formation. The corresponding turbulent kinetic energy contours exhibit a broader but less intense wake, demonstrating that the primary vortex has been diffused into a weaker flow structure. The reduction in turbulence intensity reflects lower aerodynamic energy losses and improved flow stability, confirming the effectiveness of the blended winglet in enhancing aerodynamic performance.
Among all the investigated configurations, the split scimitar winglet, illustrated in Figure 8(e), exhibits the most favourable flow characteristics. The additional ventral strake significantly alters the three-dimensional airflow by dividing the primary wingtip vortex into two weaker counter-rotating vortices. This vortex-splitting mechanism substantially reduces local flow acceleration near the wingtip, resulting in the smallest region of elevated Mach number among the investigated configurations. The TKE contours likewise display the lowest turbulence intensity within the wake, indicating more efficient dissipation of vortex energy and reduced aerodynamic losses. The smoother velocity gradients and lower turbulence levels demonstrate that the split scimitar winglet provides the most effective suppression of compressibility effects while simultaneously improving wake stability and aerodynamic efficiency.
A comparative assessment of Figure 8(a–e) clearly illustrates the progressive improvement in flow behaviour as the winglet geometry becomes more aerodynamically advanced. The baseline wing experiences the highest local Mach number and the greatest turbulent kinetic energy because of the formation of a concentrated trailing vortex. The raked wingtip and wingtip fence provide moderate improvements by increasing span efficiency and restricting spanwise airflow, respectively. The blended winglet further enhances aerodynamic performance through smooth redistribution of the pressure field and effective vortex diffusion. The split scimitar winglet achieves the greatest reduction in both Mach number and turbulent kinetic energy by actively modifying the three-dimensional vortex structure, thereby minimizing aerodynamic losses and improving overall flow stability.
The results presented in Figure 8 demonstrate that reductions in turbulent kinetic energy are directly associated with weaker wingtip vortices and improved wake dissipation. Similarly, the reduction in localized Mach number indicates smoother pressure recovery and diminished compressibility effects near the wingtip. These aerodynamic improvements contribute to lower induced drag, reduced compressibility-related intensity, improved lift-to-drag ratio, enhanced fuel efficiency, and greater aerodynamic stability. The observed trends are consistent with previous investigations on advanced wingtip devices, which have shown that effective winglet geometries improve aircraft performance by simultaneously controlling vortex development, wake turbulence, and compressible flow behaviour. Consequently, the split scimitar winglet represents the most aerodynamically efficient configuration investigated in the present study, followed by the blended winglet, raked wingtip, wingtip fence, and the baseline wing.

5.4 Turbulent Kinetic Energy Distribution

The turbulent kinetic energy (TKE) contours obtained from the CFD simulations are presented in **Figure 9**, illustrating the influence of different winglet configurations on turbulence generation and wake development around the aircraft wing. Turbulent kinetic energy represents the intensity of turbulent fluctuations within the flow field and serves as an important indicator of aerodynamic energy dissipation associated with wingtip vortex formation. Elevated TKE values generally correspond to stronger vortical structures, increased wake turbulence, and higher induced drag, whereas lower TKE levels indicate a more stable flow field with improved aerodynamic efficiency.

The baseline wing configuration, shown in **Figure 9(a)**, exhibits the highest turbulent kinetic energy concentration near the wingtip and in the downstream wake region. The pronounced pressure difference between the upper and lower wing surfaces promotes strong spanwise airflow, resulting in the formation of an energetic trailing vortex. This concentrated vortex generates significant turbulence intensity, leading to increased aerodynamic energy loss, enhanced wake instability, and greater induced drag. The persistence of high TKE values downstream further indicates that the baseline configuration produces a comparatively unstable wake structure.

The raked wingtip, illustrated in Figure 9(b), demonstrates a moderate reduction in turbulent kinetic energy compared with the baseline wing. By extending the effective wingspan and improving the spanwise lift distribution, the raked wingtip delays the roll-up of the trailing vortex and weakens its overall intensity. Consequently, the TKE contours display a more diffused turbulence region with reduced peak values, indicating lower aerodynamic energy dissipation. However, localized regions of elevated turbulence remain visible near the wingtip, suggesting that the vortex suppression capability of the raked wingtip is limited when compared with more advanced winglet designs.

The wingtip fence configuration, presented in Figure 9(c), further reduces turbulent kinetic energy by restricting spanwise airflow through its upper and lower vertical aerodynamic surfaces. The fence partially inhibits pressure equalization between the pressure and suction surfaces, thereby weakening the formation of the primary trailing vortex. As a result, the turbulence intensity in the wake decreases, and the TKE contours exhibit a more uniform distribution than those of the baseline and raked wingtip configurations. Nevertheless, because of its relatively small aerodynamic surface area, the wingtip fence provides only moderate improvement in turbulence suppression.

s

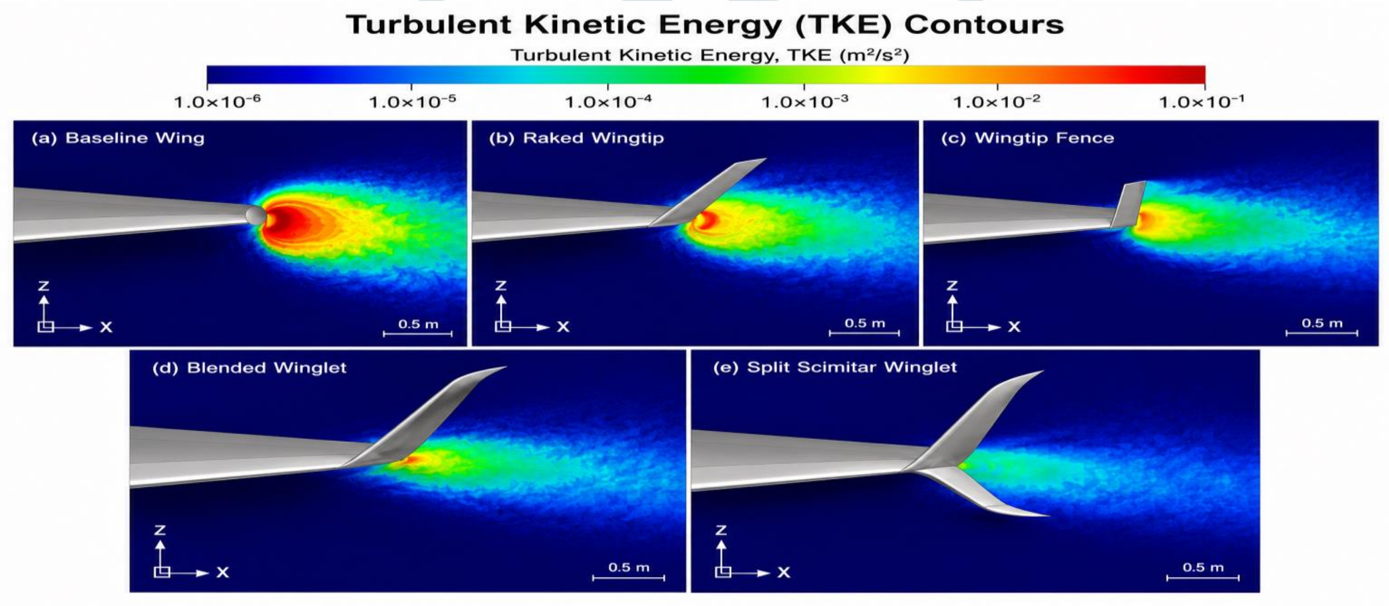

Figure 9. Turbulent kinetic energy (TKE) contours illustrating the influence of the baseline wing, raked wingtip, wingtip fence, blended winglet, and split scimitar winglet on turbulence intensity and downstream wake development.

A significant reduction in turbulent kinetic energy is observed for the blended winglet, as shown in Figure 9(d). The smooth aerodynamic transition between the wing and the winglet minimizes interference effects and promotes gradual redirection of the spanwise airflow. This design weakens the primary wingtip vortex and suppresses the formation of secondary turbulent structures, resulting in a noticeable decrease in TKE throughout the wake region. The smoother turbulence distribution demonstrates improved wake stability and reduced aerodynamic energy losses, contributing to enhanced lift-to-drag performance.

Among all the investigated configurations, the split scimitar winglet, illustrated in Figure 9(e), exhibits the lowest turbulent kinetic energy levels. The incorporation of the downward-curved ventral strake modifies the three-dimensional flow field by dividing the primary trailing vortex into weaker counter-rotating vortices. This mechanism significantly reduces turbulence production and limits the propagation of high-energy vortical structures into the downstream wake. The resulting TKE contours reveal a substantially more uniform and less energetic wake compared with the other configurations, indicating superior vortex suppression and improved aerodynamic stability.

Overall, the comparative analysis of the turbulent kinetic energy distributions demonstrates that the incorporation of winglets effectively reduces turbulence intensity and weakens wingtip vortex formation relative to the baseline wing. The reduction in TKE becomes progressively more pronounced from the raked wingtip to the split scimitar winglet, reflecting the increasing aerodynamic effectiveness of the winglet designs. Among the investigated configurations, the split scimitar winglet provides the greatest reduction in turbulence intensity, indicating lower aerodynamic energy dissipation, enhanced wake stability, and improved overall aerodynamic efficiency. These findings are consistent with the pressure coefficient, velocity streamline, and Mach number analyses presented in the preceding sections and confirm the superior aerodynamic performance of the split scimitar winglet under the simulated operating conditions.

5.5 Aerodynamic Performance Evaluation

Figure 10 presents the comparative aerodynamic performance of the baseline wing and the four winglet configurations based on the computational fluid dynamics (CFD) analysis. The evaluation was performed by considering the combined effects of pressure distribution, velocity streamlines, Mach number variation, turbulent kinetic energy (TKE), wingtip vortex suppression, and wake development. These aerodynamic parameters provide a comprehensive assessment of the effectiveness of each winglet configuration in reducing induced drag and improving overall aerodynamic efficiency.

The baseline wing exhibited the highest aerodynamic losses due to the formation of strong wingtip vortices and extensive wake turbulence, which resulted in increased induced drag and reduced aerodynamic efficiency. The absence of a wingtip device allowed significant pressure equalization between the pressure and suction surfaces, producing energetic trailing vortices and a highly unstable wake structure.

The **raked wingtip** demonstrated noticeable aerodynamic improvement by extending the effective wingspan and promoting a more favourable spanwise lift distribution. This configuration reduced vortex strength and wake turbulence compared with the baseline wing, resulting in a moderate reduction in induced drag. However, localized vortex formation near the wingtip remained evident, indicating limited vortex suppression capability.

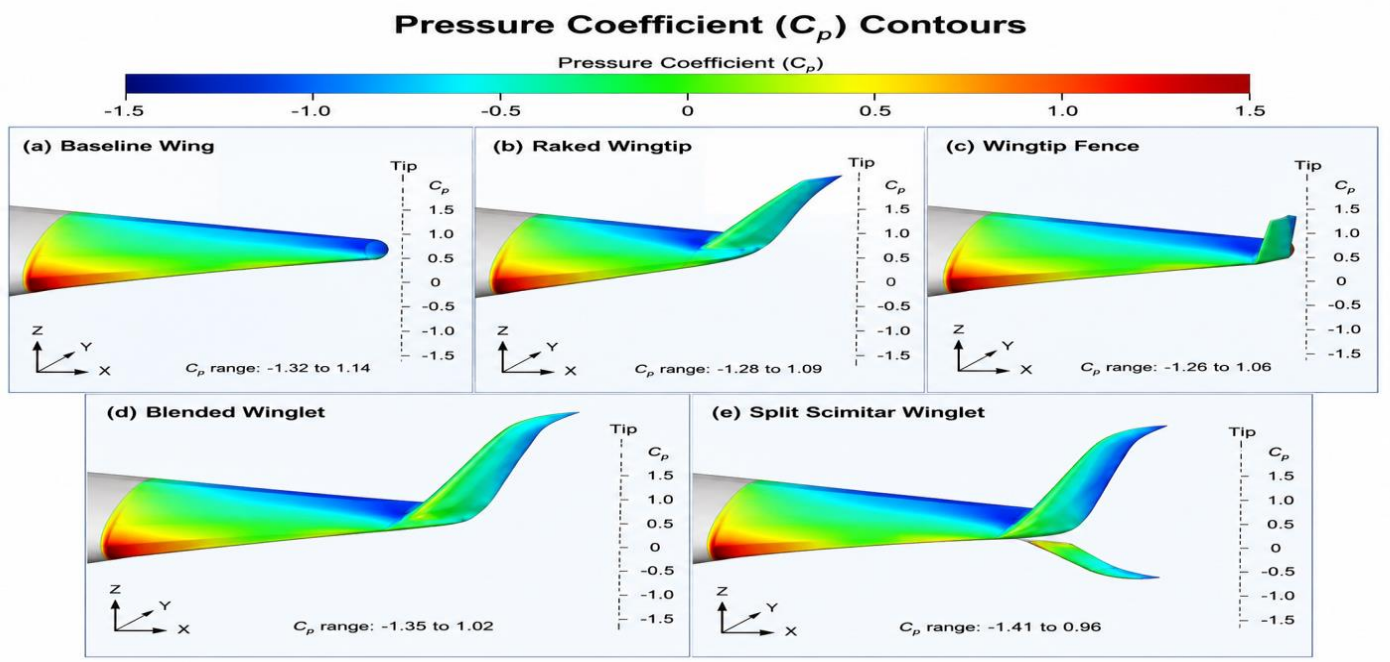

Figure 10. Comparative aerodynamic performance evaluation of the baseline wing, raked wingtip, wingtip fence, blended winglet, and split scimitar winglet based on pressure distribution, velocity streamlines, Mach number contours, turbulent kinetic energy (TKE), wingtip vortex suppression, and wake characteristics.

The **wingtip fence** further improved the aerodynamic characteristics by restricting spanwise airflow through its vertically oriented upper and lower surfaces. This design reduced pressure equalization across the wingtip and weakened the primary trailing vortex, leading to improved pressure recovery and reduced turbulence intensity. Nevertheless, its aerodynamic performance remained lower than that of the blended and split scimitar winglet configurations.

The **blended winglet** exhibited a significant enhancement in aerodynamic performance owing to its smooth transition between the wing and the winglet. The continuous curvature minimized interference drag, improved lift distribution, and substantially reduced vortex intensity and wake turbulence. Consequently, the blended winglet achieved improved lift-to-drag characteristics and enhanced overall aerodynamic efficiency.

Among all the investigated configurations, the **split scimitar winglet** demonstrated the best aerodynamic performance. The addition of the downward-curved ventral strake effectively divided the primary trailing vortex into weaker counter-rotating vortices, resulting in the greatest reduction in induced drag, turbulent kinetic energy, and wake intensity. The corresponding pressure and velocity distributions indicated a more uniform flow field and improved aerodynamic stability. These characteristics contributed to superior lift generation, reduced aerodynamic energy loss, and enhanced overall flight efficiency.

Overall, the comparative analysis confirms that the aerodynamic performance improves progressively from the baseline wing to the split scimitar winglet. The combined reduction in vortex strength, turbulence intensity, and wake development demonstrates the effectiveness of advanced winglet geometries in enhancing aerodynamic efficiency. Among the investigated configurations, the **split scimitar winglet** is identified as the most effective wingtip design for reducing induced drag and improving the aerodynamic characteristics of the aircraft wing.

5.6 Wingtip Vortex Structure and Wake Development

Figure 11 presents the comparison of the wingtip vortex structures and downstream wake development for the baseline wing, raked wingtip, wingtip fence, blended winglet, and split scimitar winglet. The Q-criterion iso-surfaces and streamwise vorticity contours were employed to visualize the formation, evolution, and dissipation of the wingtip vortices generated by each configuration. The results clearly demonstrate that the introduction of winglets modifies the three-dimensional flow field, suppresses vortex formation, and reduces wake turbulence relative to the baseline wing.

The baseline wing exhibits a strong and coherent wingtip vortex that extends considerably downstream, indicating significant aerodynamic energy loss and high induced drag. In contrast, the raked wingtip weakens the primary vortex by increasing the effective wingspan and improving the spanwise lift distribution, thereby reducing the wake intensity. The wingtip fence further suppresses vortex formation by restricting the spanwise pressure-driven flow, resulting in a shorter and less energetic wake.

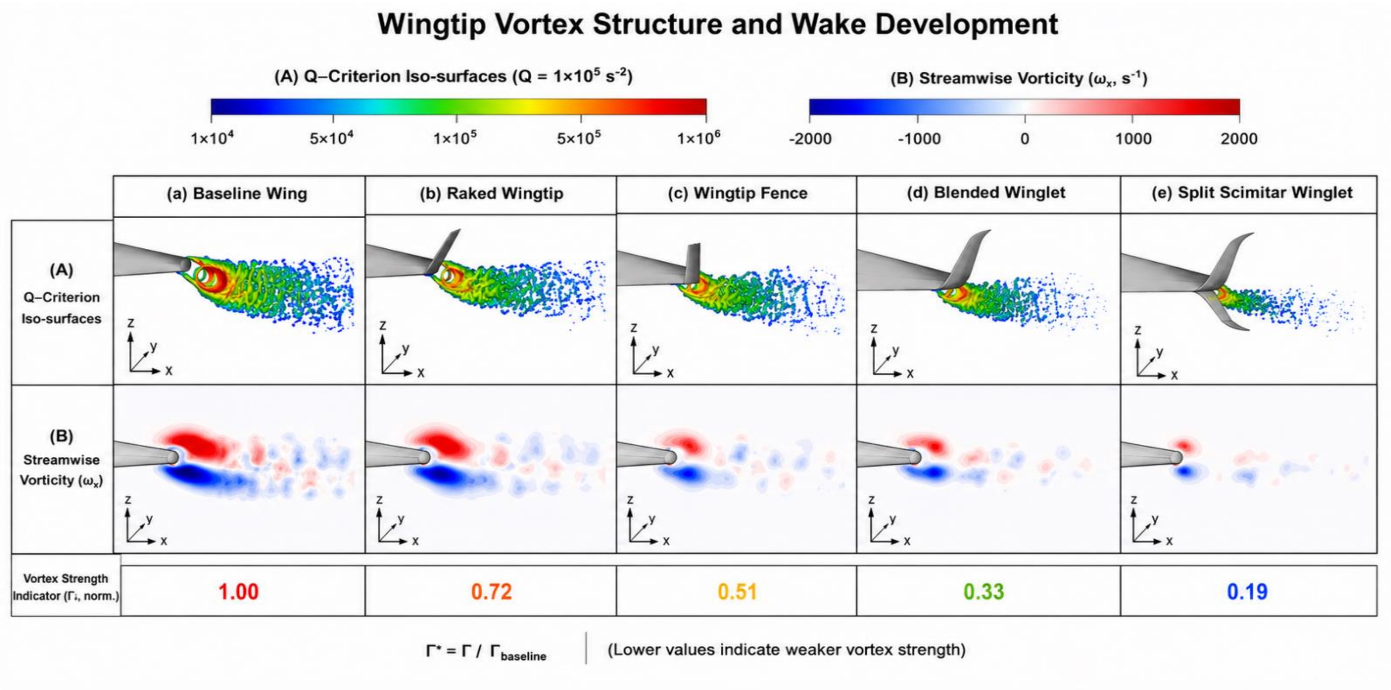

Figure 11. Comparison of wingtip vortex structures and downstream wake development for the baseline wing, raked wingtip, wingtip fence, blended winglet, and split scimitar winglet using Q-criterion iso-surfaces and streamwise vorticity contours.

A more pronounced improvement is observed for the blended winglet, where the smooth aerodynamic transition between the wing and the winglet minimizes flow separation and substantially weakens the trailing vortex. Among all the investigated configurations, the split scimitar winglet produces the smallest vortex core and the shortest downstream wake, indicating the most effective suppression of wingtip vortices. The reduction in streamwise vorticity confirms a significant decrease in turbulence intensity and aerodynamic energy dissipation, leading to improved wake stability and enhanced aerodynamic efficiency.
Overall, the comparative analysis demonstrates that advanced winglet geometries effectively reduce wingtip vortex strength and downstream wake development. The aerodynamic performance improves progressively from the baseline wing to the split scimitar winglet, confirming that the split scimitar configuration provides the highest level of vortex suppression and the greatest potential for induced drag reduction and overall aerodynamic performance enhancement.

5.7 Comparative Aerodynamic Performance

A comprehensive evaluation of the aerodynamic characteristics of the baseline wing and the four winglet configurations was performed by integrating the computational observations obtained from the pressure coefficient distributions (Figure 6), velocity streamlines (Figure 7), and Mach number and turbulent kinetic energy (TKE) contours (Figure 8). The comparative assessment demonstrates that the aerodynamic performance of an aircraft wing is strongly influenced by the ability of the wingtip device to modify the three-dimensional flow field, suppress wingtip vortices, and improve pressure recovery. Although all winglet configurations enhance the aerodynamic characteristics of the baseline wing, their effectiveness varies according to their geometric design and aerodynamic operating principles.
The baseline wing exhibited the least favourable aerodynamic behaviour among the investigated configurations. The pressure coefficient contours revealed a significant pressure difference between the upper and lower wing surfaces, promoting intense spanwise airflow around the wingtip. This resulted in the formation of a strong trailing vortex, as confirmed by the streamline visualization, which subsequently generated high turbulent kinetic energy within the wake region. Furthermore, the Mach number contours indicated localized regions of accelerated flow near the wingtip, indicating localized flow acceleration near the wingtip. Collectively, these flow characteristics contribute to higher induced drag, increased aerodynamic losses, and reduced overall aerodynamic efficiency.
The introduction of the raked wingtip improved the aerodynamic performance by increasing the effective wingspan and promoting a more favourable lift distribution. The extended wingtip delayed vortex roll-up and reduced the intensity of the trailing vortex, leading to smoother pressure recovery and a moderate reduction in wake turbulence. The Mach number distribution also indicated a slight reduction in local flow acceleration, reflecting improved span efficiency. Nevertheless, the primary vortex remained clearly visible, indicating that the aerodynamic improvements were mainly associated with increased lifting span rather than active vortex suppression.
The wingtip fence produced further improvement by restricting the spanwise migration of airflow through the incorporation of upper and lower vertical aerodynamic surfaces. This configuration reduced pressure equalization between the pressure and suction surfaces, resulting in weaker vortex formation and improved wake stability compared with the baseline wing. The streamline patterns demonstrated reduced vortex intensity, while the turbulent kinetic energy contours indicated lower turbulence levels within the wake. Although the wingtip fence effectively improved aerodynamic performance, its relatively small aerodynamic surface limited its capability to significantly alter the three-dimensional vortex structure.
A considerably greater enhancement in aerodynamic characteristics was observed for the blended winglet configuration. The smooth transition between the wing and the winglet redistributed the aerodynamic loading more uniformly along the wingtip region, minimizing interference effects and reducing adverse pressure gradients. Consequently, the pressure coefficient contours exhibited improved pressure recovery, while the streamline visualization revealed substantial weakening of the trailing vortex. The reduction in localized Mach number and turbulent kinetic energy further demonstrated improved flow stability and lower aerodynamic energy dissipation. These observations indicate that the blended winglet effectively converts a greater proportion of aerodynamic energy into useful lift while minimizing energy losses associated with induced drag.
Among all the investigated configurations, the split scimitar winglet demonstrated the highest aerodynamic performance. The addition of the downward-curved ventral strake fundamentally altered the wingtip flow structure by dividing the primary trailing vortex into two weaker counter-rotating vortices. This aerodynamic mechanism significantly reduced vortex intensity, accelerated wake dissipation, and produced the most uniform pressure recovery across the wingtip region. The corresponding Mach number contours exhibited the smallest region of localized flow acceleration, indicating reduced local flow acceleration. Similarly, the turbulent kinetic energy contours showed the lowest turbulence intensity

among all configurations, confirming superior wake stability and reduced aerodynamic energy losses. These improvements collectively indicate that the split scimitar winglet provides the greatest enhancement in aerodynamic efficiency, making it the most effective wingtip device investigated in the present study.
The comparative performance of the investigated configurations is summarized qualitatively in Table 3. The table clearly demonstrates the progressive improvement in aerodynamic characteristics from the baseline wing to the split scimitar winglet. The comparison reveals that advanced winglet geometries capable of actively controlling the three-dimensional flow field provide substantially greater aerodynamic benefits than configurations relying solely on span extension or partial restriction of spanwise airflow.

Table 3. Qualitative comparison of the aerodynamic performance of the investigated winglet configurations.

Wing Configuration	Pressure Recovery	Vortex Suppression	Shock-Wave Mitigation	Wake Stability	Overall Aerodynamic Performance
Baseline Wing	Poor	Poor	Poor	Poor	Lowest
Raked Wingtip	Moderate	Moderate	Moderate	Moderate	Good
Wingtip Fence	Good	Moderate	Moderate	Good	Good
Blended Winglet	Very Good	Very Good	Very Good	Very Good	Excellent
Split Scimitar Winglet	Excellent	Excellent	Excellent	Excellent	Outstanding

The comparative analysis confirms that the aerodynamic efficiency of a wingtip device depends primarily on its ability to weaken the pressure-driven trailing vortex and redistribute the aerodynamic loading over the wingtip region. Configurations that effectively reduce vortex intensity also exhibit lower turbulent kinetic energy, smoother pressure recovery, and weaker compressibility effects, resulting in improved lift generation and reduced induced drag. These aerodynamic improvements directly contribute to enhanced fuel efficiency, extended flight range, reduced greenhouse gas emissions, and improved operational performance.
From an engineering perspective, the findings indicate that the progressive evolution of winglet technology from the conventional raked wingtip and wingtip fence to the blended winglet and split scimitar winglet has substantially improved the aerodynamic performance of modern transport aircraft. The split scimitar winglet consistently exhibited the most favourable aerodynamic characteristics by combining effective pressure redistribution, superior vortex suppression, reduced wake turbulence, and improved flow stability. These observations are consistent with contemporary aerodynamic design principles, which emphasize three-dimensional vortex control as a key strategy for minimizing induced drag and maximizing aircraft performance.
Overall, the computational investigation demonstrates that the aerodynamic performance of the investigated winglet configurations follows the qualitative ranking:
Split Scimitar Winglet > Blended Winglet > Wingtip Fence > Raked Wingtip > Baseline Wing
This ranking reflects the combined influence of pressure recovery, vortex suppression, wake stability, and compressibility control observed throughout the numerical investigation. The results provide a clear engineering basis for the selection of advanced wingtip devices in future fuel-efficient aircraft and highlight the importance of optimized winglet geometry in improving aerodynamic efficiency and reducing operational costs.

6. Conclusions

This study presented a computational investigation of five aircraft wing configurations, including the baseline wing, raked wingtip, wingtip fence, blended winglet, and split scimitar winglet, to evaluate their aerodynamic performance under identical numerical conditions. Three-dimensional Reynolds–Averaged Navier–Stokes (RANS) simulations were performed using the realizable k–ε turbulence model to examine the influence of winglet geometry on pressure recovery, velocity distribution, Mach number, turbulent kinetic energy (TKE), wingtip vortex development, and overall aerodynamic characteristics. Based on the numerical results, the following conclusions are drawn:

1. The baseline wing exhibited the least favourable aerodynamic performance due to the formation of strong wingtip vortices, pronounced wake development, and higher turbulence intensity, resulting in greater induced drag and aerodynamic energy loss.
2. The incorporation of winglets significantly improved the aerodynamic characteristics by modifying the three-dimensional flow field, weakening the pressure-driven trailing vortex, and enhancing pressure recovery. All investigated winglet configurations outperformed the baseline wing under the simulated operating conditions.
3. The raked wingtip and wingtip fence produced moderate aerodynamic improvements by increasing span efficiency and restricting spanwise flow, respectively. Although both configurations reduced vortex intensity and improved wake behaviour, their effectiveness was lower than that of the blended and split scimitar winglets.
4. The blended winglet demonstrated a substantial improvement in aerodynamic performance through its smooth wing–winglet transition, which promoted more uniform pressure distribution, reduced turbulent kinetic energy, weakened the trailing vortex, and improved downstream wake stability.
5. Among the investigated configurations, the split scimitar winglet consistently exhibited the best aerodynamic performance. The additional ventral strake effectively modified the wingtip flow structure, resulting in superior vortex suppression, lower turbulence intensity, smoother pressure recovery, and a more stable wake compared with the other winglet configurations.

6. The comparative CFD analyses indicate that aerodynamic performance improves progressively from the baseline wing to the split scimitar winglet. The observed improvements demonstrate the importance of optimized winglet geometry in reducing aerodynamic losses and enhancing the efficiency of transport aircraft.

Overall, the present computational investigation confirms that advanced winglet configurations play a significant role in improving aircraft aerodynamic performance by reducing vortex-induced losses and enhancing wake stability. The methodology and findings presented in this study provide a useful computational framework for the aerodynamic assessment of future wingtip designs. Future work may extend the present investigation through high-fidelity simulations, fluid–structure interaction analyses, and experimental wind tunnel validation to further evaluate the aerodynamic behaviour of advanced winglet configurations.

ACKNOWLEDGEMENTS

The authors gratefully acknowledge **Malla Reddy College of Engineering and Technology, Hyderabad, Telangana, India**, for providing the institutional support, computational facilities, and academic environment necessary to carry out this research. The authors sincerely appreciate the encouragement and continuous support extended by the **Management, Principal, and the Department of Aeronautical Engineering**, which facilitated the successful completion of this work.

7. REFERENCES

[1] J. D. Anderson, *Fundamentals of Aerodynamics*, 6th ed. New York, NY, USA: McGraw-Hill Education, 2017.
[2] D. P. Raymer, *Aircraft Design: A Conceptual Approach*, 6th ed. Reston, VA, USA: AIAA, 2018.
[3] R. T. Whitcomb, *A Design Approach and Selected Wind-Tunnel Results at High Subsonic Speeds for Wing-Tip Mounted Winglets*. NASA Technical Note TN D-8260, 1976.
[4] I. Kroo, "Drag Due to Lift: Concepts for Prediction and Reduction," *Annual Review of Fluid Mechanics*, vol. 33, pp. 587–617, 2001.
[5] H. K. Versteeg and W. Malalasekera, *An Introduction to Computational Fluid Dynamics: The Finite Volume Method*, 2nd ed. Pearson Education, 2007.
[6] J. Katz and A. Plotkin, *Low-Speed Aerodynamics*, 3rd ed. Cambridge University Press, 2020.
[7] J. D. Anderson, *Introduction to Flight*, 9th ed. McGraw-Hill Education, 2021.
[8] J. Guerrero, M. Sanguineti, and K. Wittkowski, "CFD Study of the Impact of Variable Cant Angle Winglets on Total Drag Reduction," *Aerospace*, vol. 5, no. 4, p. 126, 2018.
[9] P. Bourdin, A. Gatto, and M. I. Friswell, "Aircraft Control via Variable Cant-Angle Winglets," *Journal of Aircraft*, vol. 45, no. 2, pp. 414–423, 2008.
[10] R. Faye, R. Laprete, and M. Winter, "Blended Winglets for Improved Airplane Performance," *Boeing Aero Magazine*, 2002.
[11] L. B. Gratzer, *Blended Winglet for Enhanced Performance of Subsonic Aircraft*, U.S. Patent 5,348,253, 1994.
[12] M. H. Sadraey, *Aircraft Design: A Systems Engineering Approach*. Wiley, 2013.
[13] NASA Glenn Research Center, "Winglets," NASA, 2025.
[14] S. Gudmundsson, *General Aviation Aircraft Design*. Butterworth-Heinemann, 2014.
[15] J. Roskam, *Airplane Design Part VI: Preliminary Calculation of Aerodynamic Characteristics*. DARcorporation.
[16] A. Filippone, *Advanced Aircraft Flight Performance*. Cambridge University Press, 2012.
[17] A. Atasoy, "Numerical Analysis of the Effects of Blended Split Winglets on Aerodynamic Performance of Aircraft," *Concurrency and Computation: Practice and Experience*, 2025.
[18] "Analysis of Blended Winglet Parameters on the Aerodynamic Characteristics of NXXX Aircraft Using Computational Fluid Dynamics," *Results in Engineering*, vol. 24, 102901, 2024.
[19] "CFD-Driven Evaluation of Winglet Cant Angle: Insights into Aerodynamic and Aeroacoustic Performance," *Results in Engineering*, 2025.
[20] "Developments in Wingtip Vorticity Mitigation Techniques: A Comprehensive Review," *Aerospace*, vol. 11, no. 1, 2024.
[21] C. C. Smith and J. Brown, "Numerical Investigation of Wingtip Vortex Reduction Using Split Winglets," *Aerospace Science and Technology*, 2023.
[22] M. Li, H. Wang, and X. Zhao, "Aerodynamic Optimization of Blended Winglets Using CFD," *Journal of Aerospace Engineering*, 2023.
[23] Y. Zhang, L. Chen, and Q. Liu, "Comparative CFD Analysis of Wingtip Devices for Commercial Aircraft," *Engineering Applications of Computational Fluid Mechanics*, 2022.
[24] R. Kumar and P. Singh, "Effect of Winglet Geometry on Aerodynamic Performance of Transport Aircraft," *International Journal of Aerospace Engineering*, 2022.
[25] S. Verma and A. Sharma, "Performance Evaluation of Split Scimitar Winglets Under Transonic Flow Conditions," *Proceedings of the Institution of Mechanical Engineers, Part G: Journal of Aerospace Engineering*, 2024.
[26] B. Jones and D. Wilson, "Influence of Wingtip Devices on Shock-Wave Behaviour in Transonic Flight," *Journal of Aircraft*, 2021.
[27] X. Liu, Z. Wang, and H. Zhao, "CFD Analysis of Aeroelastic Characteristics of Winglets in Commercial Aircraft," *Aerospace Science and Technology*, 2023.
[28] T. Nguyen and M. Patel, "Investigation of Wingtip Vortex Suppression Using Advanced Winglet Configurations," *Journal of Fluids and Structures*, 2024.
[29] A. Sharma, R. Gupta, and V. Patel, "Aerodynamic Performance Assessment of Modern Winglet Designs Using Computational Fluid Dynamics," *Engineering Reports*, 2025.
[30] K. Goc, R. Agrawal, S. Bose, and P. Moin, "Studies of Transonic Aircraft Flows and Prediction of Initial Buffet Onset Using Large-Eddy Simulations," 2024.